

## THERMAOPHYSICAL PROPERTIES OF BORON PHOSPHIDE SINGLE CRYSTALLINE WAFERS

Y. Kumashiro

*Department of Material Science and Chemical Engineering, Yokohama National University, Hodogaya-ku, Yokohama, 240, Japan*

The present article describes thermophysical properties of well-characterized boron phosphide single crystalline wafers prepared using chemical vapor deposition up to high temperatures. The thermal diffusivity was measured by using unique ring flash light method. It has large value of  $1.8 \text{ cm}^2/\text{sec}$  at room temperature and shows pronounced decrease in raising temperature due to phonon scattering. Analysis of specific heat capacity by differential scanning calorimetry method induces Debye temperature, and Grüneisen parameter, which demonstrate low atomic mass, strong interatomic bonding, low anharmonicity and low ionicity in boron phosphide. The thermal conductivity calculated by the products of thermal diffusivity, specific heat capacity and density of the wafer produces high thermal conductivity of  $4.0 \text{ W-cm-K}$  at room temperature and is comparable to that of boron nitride. Boron phosphide single crystal is a promising material for heat-sink substrate for semiconductor device. Temperature dependence of thermal conductivity almost coincides with calculated lattice thermal conductivity by 3-phonon processes. Also promising thermoelectric properties employing sintered polycrystal disc are mentioned briefly.

### Introduction

The III-V compound semiconductors are attractive for thermal conductivity studies. These materials offer a wide range of lattice and electronic properties. They can be obtained in highly pure form, so that impurity effects are minimized and the intrinsic properties can be investigated and compared.

Thermal conductivity is also of technological importance. The thermal conductivity value is necessary in calculating the figure of merit for thermoelectric devices. For power dissipating devices such as diodes, transistors, or lasers it is useful to know the value of the thermal conductivity to assist in device and circuit design.

Boron phosphide (BP), one of the III-V compound semiconductors with a wide band gap is a promising material for application in thermoelectric device operating at high temperatures.

The constituent atoms of BP are light elements and especially boron belongs to first law of III group of periodic table with small inner shells. Then the characteristics of boron phosphide are summarized as follows.

- (1) BP forms tetragonal bonded structure with small lattice constant and exhibits strong covalent bonding with small ionicity.
- (2) BP is mechanically strong and has elastic constant as large as  $\beta$ -SiC.
- (3) BP has high melting point, high Debye temperature and high thermal conductivity which make high thermal and chemical stabilities.

- (4) BP has wide band gap with indirect transition.
- (5) The unharmonicity of the lattice is large in comparison with other conventional semiconductors.

Then the thermal conductivity of BP is important to determine thermoelectric figure of merit. However there are two reports, i.e., single crystalline wafer above room temperature [1] and small single crystal below room temperature [2]. However, the thermal conductivities at room temperature differ by two orders of magnitude [3]. Then main object of the present paper [4, 5] lies in the measurement of thermal diffusivity by modified laser flash method, because the conventional laser flash method many problems to apply to thick wafers. The present article describes the electric and thermal characteristics of well-characterized boron phosphide single crystalline wafers made by CVD process [6] to clarify intrinsic thermophysical properties.

### Theoretical

The specific heat gives the value of Debye temperature  $\theta$ , and Grüneisen parameter  $\gamma$  which are important parameters for the phenomena involving the lattice vibrations such as electrical resistivity and thermal conductivity.  $\theta$  is obtained from the specific heat at constant volume  $C_v$ , which is deduced by the usual thermodynamic formula

$$C_v = C_p - (\beta^2 V / K) T \quad (1)$$

where  $\beta = 3\alpha$  is the coefficient of volume expansion,  $K$  the isothermal compressibility, and  $V$  the

molar volume. With the value [7] of  $K=5.3 \times 10^{-13} \text{ cm}^2 \cdot \text{dyn}^{-1}$ ,  $V=14.07 \text{ cm}^3 \cdot \text{mol}^{-1}$  and the published data on  $\alpha$  [8],  $C_p$  is converted to  $C_v$ .  $\beta$  is calculated by the following formula

$$C_v/6R = (3/x^3) \int_0^x [x^4 e^x / (e^x - 1)^2] dx \quad (2)$$

$$x = \theta/T \quad (3)$$

where  $R$  is the gas constant of  $1.987 \text{ cal} \cdot \text{mol}^{-1} \cdot \text{K}^{-1}$ . The values of the right term in Eq. (2) are tabulated [9].

$\gamma$  is calculated by the following formula

$$\gamma = \beta V / KC_v = 3\alpha V / KC_v \quad (4)$$

We have solved difficulty in laser flash method to measure the thermal diffusivity of a wafer by using a ring flashlight, which originates from many-variable analysis in a two-dimensional model. Details of this method will be described elsewhere [10]. We mention only outline. Here we consider the cylindrical coordinate for homogeneous cylinder as is shown in Fig. 1,  $r_0$  indicates the region where temperature is measured. When laser light irradiates the specimen in the form of a ring with inner radius  $r_1$  and outer radius,  $r_2$  the temperature from the central axis to the radius, of the disk  $T(x, r, t)$  can be derived from general solutions of heat conduction equations for cylindrical samples [11], and is given by

$$T(x, r_0, t) = T_0 \sum Y_i(x) Y_i(0) \sum H_j(r_0) G_j \exp(-C_{ij}t) \quad (5)$$

$$Y_1(x) = 2^{1/2} (\beta_i^2 + L_2^2)^{1/2} [\beta_i \cos \beta_i(x/b) + L_1 \sin \beta_i(x/b)] / b^{1/2} \{ (\beta_i^2 + L_1^2)(\beta_i^2 + L_2^2 + L_2) + L_1(\beta_i^2 + L_2^2) \}^{1/2} \quad (6)$$

$$G_j = (2a/Z_j)(r_2 J_1(Z_j r_2/a) - r_1 J_1(Z_j r_1/a)) / (r_2^2 - r_1^2) \quad (7)$$

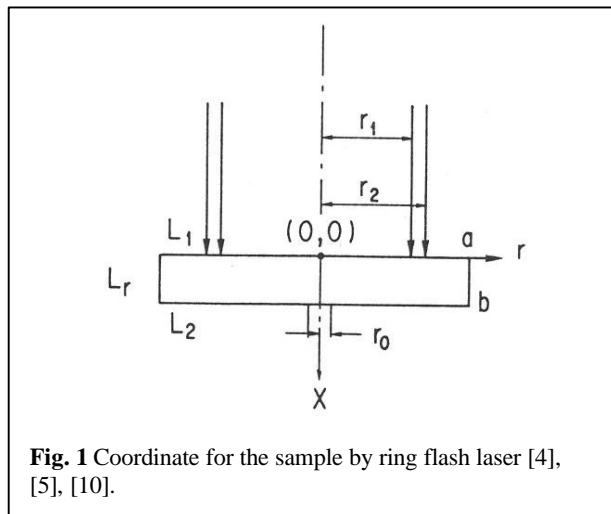


**Fig. 1** Coordinate for the sample by ring flash laser [4], [5], [10].

$$H_j(r_0) = (2aZ_j/r_0) J_1(Z_j r_0/a) / (Z_j^2 + L_r^2) J_0^2(Z) \quad (8)$$

$$C_{ij} = -\alpha(Z_j^2/a^2 + \beta_i^2/b^2) \quad (9)$$

$$\tan(\beta_i) = \beta_i(L_1 + L_2) / (\beta_i^2 - L_1 L_2) \quad (10)$$

$$Z_j J_1(Z_j) - L_r J_0(Z_j) = 0 \quad (11)$$

where  $T_0 = Q / C_p \pi^{ab}$  and  $\kappa = \alpha \rho C$ .  $J_0$  and  $J_1$  are 0<sup>th</sup> and 1<sup>st</sup> order Bessel functions, respectively,  $\beta_i$  and  $Z_j$  are positive roots of Eqs. (6) and (7), respectively,  $\alpha$ ,  $\kappa$ ,  $\rho$ ,  $C$ ,  $Q$ , and  $L_m$  represent thermal diffusivity, thermal conductivity, density, specific heat capacity, energy of disk and dimensionless number of heat loss ( $m = 1$ : irradiating face,  $m = 2$ : rear face and  $r$ : the side), respectively.

## Experimental

The BP wafers [6] were grown on (100)-, and (111)-oriented Si substrates by thermal decomposition of diborane (1% in hydrogen) and phosphine (5% in hydrogen) in a hydrogen atmosphere (3 l/min) at 950°C and 1050°C for Si (100), and 1000°C for Si (111). The growth was made at gas-flow rates of 20 or 60, 300 or 500, and 3000 cm<sup>3</sup>/min for diborane, phosphine, and hydrogen respectively in these temperatures at deposition time of 24-28 hrs. BP wafers with the area of 10 x 20 mm<sup>2</sup>, thickness of 200-300  $\mu\text{m}$ , were obtained by solving away the Si substrate in an HF-HNO<sub>3</sub> solution.

The results of the SIMS analysis [12] indicate that the majority of the impurities consist of silicon. In addition to sodium, potassium, calcium

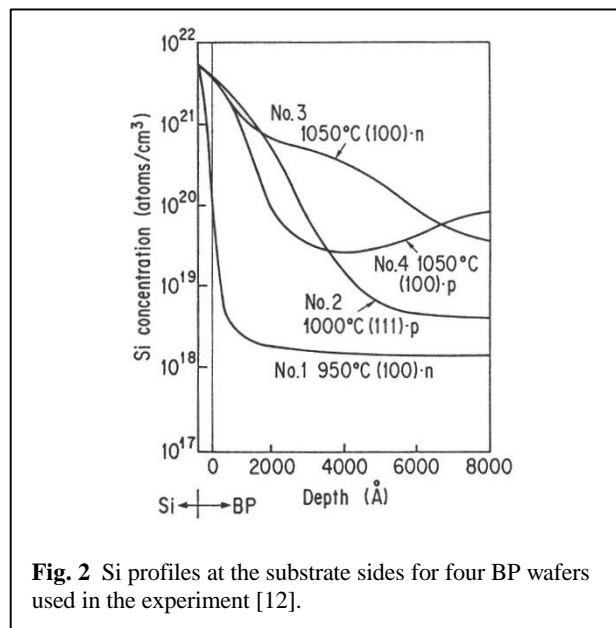


**Fig. 2** Si profiles at the substrate sides for four BP wafers used in the experiment [12].

and chromium, special impurities such as manganese, cobalt and magnesium were detected in sample 3, magnesium, titanium, vanadium, manganese and cobalt in sample 2 and manganese, cobalt and nickel in sample 4, with concentrations of the order of  $\sim 10^{15}$  atoms·cm<sup>-3</sup>.

The silicon profiles as the substrate side of the samples show that autodoping of silicon from the substrate occurs and they give an indication of the dependence of autodoping on the growth temperature and on the type of substrate plane as is represented in Fig. 2. Silicon contamination in the *n*-type wafer grown at 950°C (sample 1) is small with the exception of the first 800 Å adjacent to the silicon substrate. Samples 1, 2, 3, and 4 were found to have silicon concentrations of  $\sim 10^{18}$ ,  $5 \times 10^{18}$ ,  $5 \times 10^{19}$ , and  $\sim 10^{20}$  atoms·cm<sup>-3</sup> respectively.

The electrical resistivity  $\rho$ , carrier concentration  $n$  and mobility  $\mu$  measured by van der Pauw method are shown in Table 1. The carrier concentration decreases with increasing silicon content for the *n*-type specimens (samples 1 and 3) and increases for the *p*-type materials (samples 2 and 4). This indicates that silicon atoms act as acceptors and are incorporated at the phosphorus sites in BP.

The results of the measurements of the lattice constants by Bond method are shown in Table 2; They were obtained after calibration using the thermal expansion coefficient [12]. The conduction types of the BP wafers were determined by excess boron or phosphorus; they were found to be either *p* or *n*-type [12]. The excess phosphorus atoms occupy the boron sites in the BP lattice in

**Table 1** Semiconducting properties of BP wafers [12].

Orientation	Type	$\rho(\Omega\text{cm})$	$n(\text{cm}^{-3})$	$\mu(\text{cm}^2\cdot\text{s}^{-1}\cdot\text{V}^{-1})$
No. 1 (100)	<i>n</i>	0.15	$3.7 \times 10^{17}$	120
No. 2 (111)	<i>p</i>	12.5	$1.5 \times 10^{15}$	36.5
No. 3 (100)	<i>n</i>	2.5	$2.5 \times 10^{16}$	107
No. 4 (100)	<i>p</i>	10.0	$3.1 \times 10^{16}$	20.0

**Table 2** The precise lattice constant of BP wafers [13].

Orientation	Type	Reflection	Half band width	Lattice constant (Å)
No. 1 (100)	<i>n</i>	(400)	0.13°	$4.538675 \pm 3 \times 10^{-6}$
No. 2 (111)	<i>p</i>	(333)	0.14°	$4.537983 \pm 3 \times 10^{-6}$
No. 3 (100)	<i>n</i>	(400)	0.15°	$4.538467 \pm 7 \times 10^{-6}$
No. 4 (100)	<i>p</i>	(400)	0.14°	$4.538205 \pm 6 \times 10^{-5}$

the *n*-type material and vice versa for the *p*-type materials [12]. The ionic radii of boron and phosphorus in BP are expected to be 0.88 and 1.10 Å respectively. The lattice shrinks in the *p*-type materials (sample 4), whereas it expands in the *n*-type materials (sample 3). Sample 1 has more excess phosphorus atoms than sample 3 and has a greater lattice expansion than sample 3. Sample 2 has more excess boron atoms than sample 4 and has a greater lattice contraction than sample 4.

Specific heat capacity [4], [5] was measured on small wafers (4 x 4mm<sup>2</sup>) of boron phosphide by differential scanning calorimetry (Perkin-Elmer, DSC-2) in the temperature range of 60°-500°C with the use of automatic data processing and calibration procedures.

The process of calculating the thermal diffusivity [4,5] is as follows, firstly, known parameters  $a$ ,  $b$ ,  $r$ ,  $i$  and  $j$  are specified by measuring conditions. Secondly, initial values of unknown parameters such as  $\alpha$ ,  $T_0$  and  $L_m$  are presented. Finally, after identifying values of  $\beta_i$  and  $Z_j$ , the unknown parameters were estimated by curve fitting.

The measurements were performed on graphite and sapphire with a thickness of 0.5 mm and an area of 10 x 10mm<sup>2</sup> to confirm that they coincide with standard literature values. Graphite coated thin films with a thickness of  $\sim 5 \mu\text{m}$  were sprayed on both faces of the specimen by dry

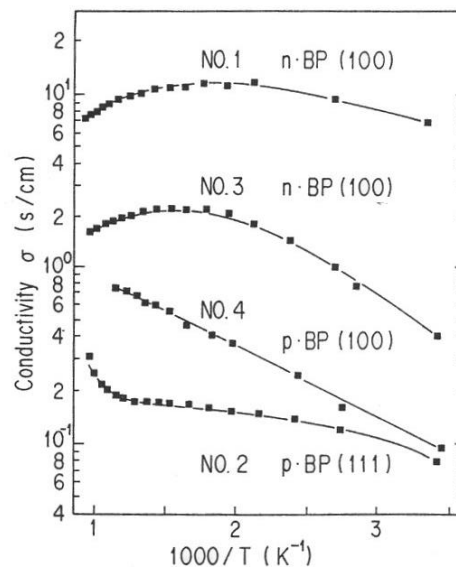


**Fig. 3** Temperature dependence of electrical conductivity of four BP wafers [5].

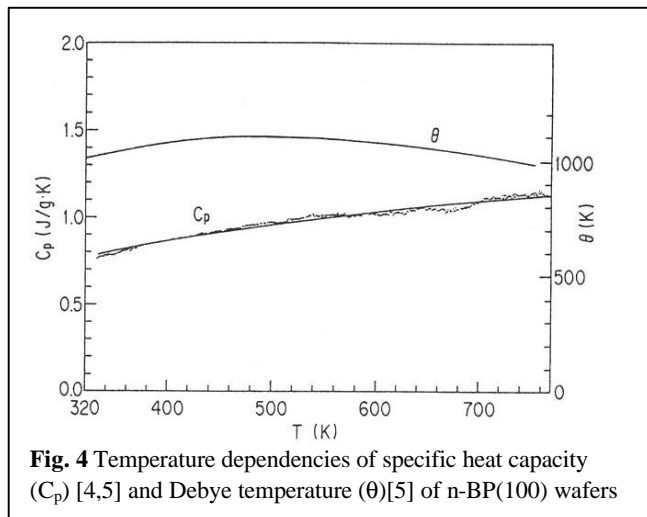


**Fig. 4** Temperature dependencies of specific heat capacity ( $C_p$ ) [4,5] and Debye temperature ( $\theta$ )[5] of n-BP(100) wafers

graphite film lubricant (dof 123).

### Results and Discussions

The temperature dependence of conductivity  $\sigma$  are shown in Fig. 3. The electric conductivity of wafers of n-types increases with temperature, becomes constant, and then begins to decrease with temperature; this can be understood as the result of a competition between decrease of mobility and the increase of carrier concentration [13]. The behavior for the p-type wafers is different: the conductivity increases with temperature, and upon further increase of temperature the intrinsic conduction region is reached.

Fig. 4 shows the specific heat capacity of n-type, (100) plane boron phosphide wafer, denoted n-(100). The specific heat capacity increases with increasing temperature, but no appreciable difference was observed between (100) and (111) planes of between p-type and n-type. If multiple regression analysis is applied to the data, the best fit is given by

$$C_p(\text{cal}\cdot\text{mol}^{-1}\cdot\text{K}^{-1}) = 4.1017 + 1.2579 \times 10^{-2}(T/\text{K}) - 2.9171 \times 10^{-6}(T/\text{K})^2 \quad (12)$$

for n-(100) wafer, and by

$$C_p(\text{cal}\cdot\text{mol}^{-1}\cdot\text{K}^{-1}) = 2.8105 + 1.8071 \times 10^{-2}(T/\text{K}) - 9.3608 \times 10^{-6}(T/\text{K})^2 \quad (13)$$

for p-(111) wafer

The temperature dependence of  $\theta$  is also shown in Fig. 4. Ohsawa et al. [7] obtained a Debye temperature of  $960 \pm 50$  K at 300 K by measuring specific heat capacity using AC calorimetry. The difference in Debye temperatures between theirs and ours would be caused by the measure-

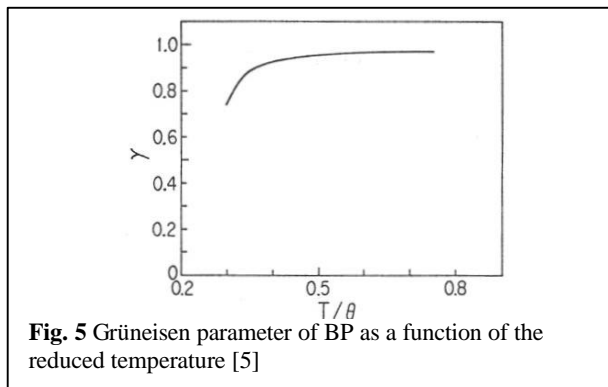


**Fig. 5** Grüneisen parameter of BP as a function of the reduced temperature [5]

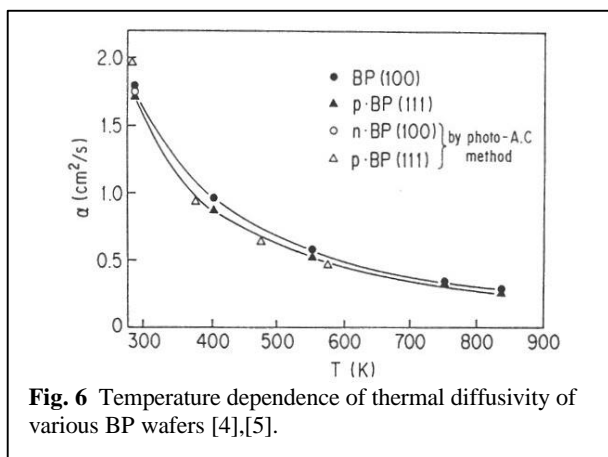


**Fig. 6** Temperature dependence of thermal diffusivity of various BP wafers [4],[5].

ment method used. The Debye temperature and its temperature dependence of the present crystal should exhibit feature of boron phosphide. High Debye temperature reflects low atomic mass and strong interatomic bonding in boron phosphide. Figure 5 shows  $\gamma$  as a function of reduced temperature  $T/\theta$ . Large  $\gamma$  means high anharmonicity and the small variation would be attributed to its low ionicity.

Temperature dependencies of thermal diffusivity together with that obtained by photo-AC method are shown in Fig. 6. A fairly good agreement between the two methods is established, which justifies the present ring flash light method. The thermal diffusibility has a large value of  $1.8 \text{ cm}^2 \cdot \text{s}^{-1}$  at room temperature and shows a pronounced decrease with increasing temperature due to phonon scattering.

The temperature dependence of thermal conductivity as calculated from the product of the thermal diffusivity (Fig. 6), specific heat capacity (Fig. 4) and density (Table 2) is shown in Fig. 7. The thermal conductivity of BP single crystalline wafers is  $\sim 4.0 \text{ W} \cdot \text{cm}^{-1} \cdot \text{K}^{-1}$  at room temperature,

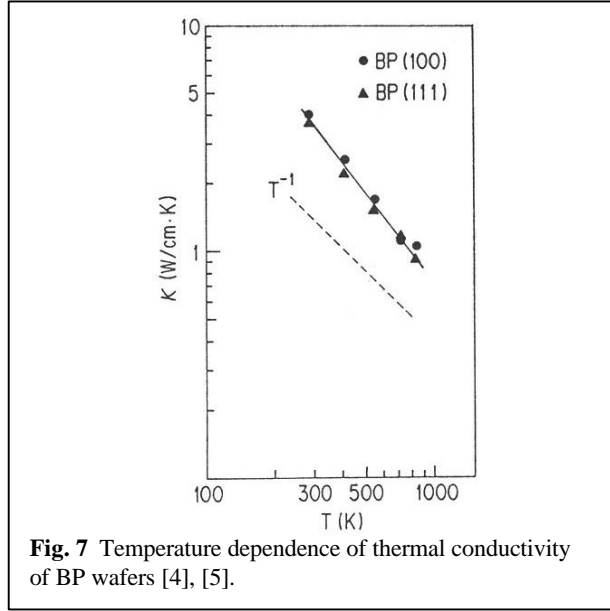


**Fig. 7** Temperature dependence of thermal conductivity of BP wafers [4], [5].

which is in good agreement with Slack's data [2] and is comparable to that of boron nitride. The high thermal conductivity of boron phosphide is similar to that of other adamantine compounds [2]. Boron phosphide is thus a promising material for heat-sink substrates for semiconductor devices. In the present single crystalline wafer the phonon scattering predominates so that thermal conductivity decreases with increasing temperature with a slope of  $\log \kappa$  vs  $\log T$  plot close to -1.

Finally, we discuss electronic and phonon contributions to heat conduction [14]. We treat the boron phosphide wafer as a nondegenerate semiconductor in considering its electrical properties (Table 1) and impurity concentrations. The electronic thermal conductivity for one sign of charge carrier is given by

$$\kappa_{el} = \left\{ \frac{z+7/2}{z+5/2} F_{z+5/2}(\xi) / \left( \frac{z+3/2}{z+1/2} F_{z+1/2}(\xi) - \left[ \frac{z+5/2}{z+3/2} F_{z+3/2}(\xi) / \frac{z+1/2}{z+3/2} F_{z+1/2}(\xi) \right]^2 \right) \right\} \cdot (k/e)^2 \sigma T = L \sigma T \quad (14)$$

where  $F_n(\xi)$  is the Fermi integral,  $k$  is Boltzmann's constant,  $e$  is the electronic charge, and  $L = [(z+5/2)(k/e)^2]$  is the Wiedemann-Franz constant and ranges between  $2(k/e)^2$  and  $4(k/e)^2$  depending on reduced Fermi level  $\xi$  and scattering parameter  $z$ .  $\sigma = 10 \Omega^{-1} \cdot \text{cm}^{-1}$  and  $T = 1000\text{K}$  (Fig. 3),  $\kappa_{el}$  of  $\sim 10^{-4} \cdot \text{W cm}^{-1} \cdot \text{K}^{-1}$ . In the case where both electrons and holes are present, in comparable numbers, the total thermal conductivity  $\kappa_{t,el}$  is given by [14]

$$\kappa_{t,el} = L_t \sigma T \quad (15)$$

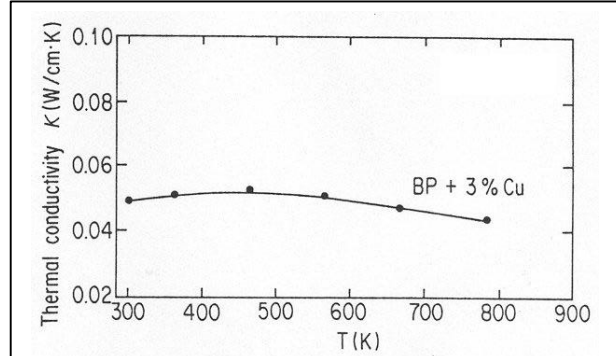


**Fig. 8** Temperature dependence of thermal conductivity of Cu 3% doped BP sintered disc [12].

where  $\sigma_t$  is total electronic conductivity  $\sigma_t = \sigma_e + \sigma_h$   $L_t$  is given by

$$L_t = (k/e)^2 (\sigma_e \sigma_h / \sigma_t^2) (E_g/kT + \alpha_e + \alpha_h)^2 + L_e \sigma_e / \sigma_t + L_h \sigma_h / \sigma_t \quad (16)$$

where  $L_e$  and  $L_h$  are the electron and hole Lorenz numbers, respectively, and  $\alpha_e$  and  $\alpha_h$  are given by  $\alpha = z + 5/2$ . When  $\sigma_e \sim \sigma_h$ ,  $E_g = 84kT$  and appropriate values of  $z$  are  $z = -1/2$  for lattice scattering,  $z = 3/2$  for impurity scattering.

With  $L_t \sim 1800 (k/e)^2$ ,  $\sigma = 3 \Omega^{-1} \cdot \text{cm}^{-1}$  and  $T = 1000\text{K}$  (Fig. 3), we found  $\kappa_{t,el} \sim 10^{-2} \text{W} \cdot \text{cm}^{-1} \cdot \text{K}^{-1}$ , which is two orders of magnitude higher than the value for one carrier. In any case electronic contribution to thermal conductivity is small, and the thermal conductivity in Fig. 7 should correspond to lattice thermal conductivity.

The lattice thermal conductivity for 3-phonon processes at high temperatures is given by [15]

$$\kappa_1 = (3/5) 4^{1/3} (k/h)^3 M \delta \theta^3 / \gamma^2 T \quad (17)$$

where  $M$  is the mean atomic mass,  $\delta$  is the cubic root of the atomic volume,  $\kappa_1$  is calculated by the values of  $\theta$  (Fig. 4) and  $\gamma$  (Fig. 5). The result is shown in Fig. 7 as a solid line is in very good agreement with the experimental result, so that thermal conduction should be limited by 3-phonon processes.

Single crystalline wafer has comparatively high thermoelectric power of 400-500  $\mu\text{V/K}$  [13], but the thermal conductivity is also high (Fig. 7), which reduces thermoelectric figure of merit. Then BP single crystalline wafer is not applicable for thermoelectric device.

The thermoelectric power of BP sintered specimen, however, depends on the purity of starting powder. Commercial available BP powder

contains much impurities, which compensate each other reducing the thermoelectric power down to  $\sim 20\mu\text{V/K}$  at entire temperature range [16].

Then we have prepared high purity BP powders by hydroisostatic pressing [12]. In doping Si, Ag and Cu to BP powder, the specimens were sintered. The thermoelectric powder of BP sintered specimen shows as high as single crystalline wafer. Especially the specimen doped with Cu 3% indicates the highest thermoelectric power of  $\sim 1.5\text{ mV/K}$  ever not reported [12].

The thermal conductivity (Fig. 8) is lower than that of single crystalline wafer (Fig. 7) by two orders of magnitude and shows weak temperature dependence, indicating that the phonon scattering at grain boundary predominates and mean free path of phonon shows weak temperature dependence.

It is demonstrated that BP sintered specimen doped with Cu 3% shows maximum thermoelectric figure of merit, i.e.,  $1.0 \times 10^{-5}/\text{K}$  at room temperature [12], being compatible to  $\text{FeSi}_2$  with  $2.4 \times 10^{-4}/\text{K}$ .

This study was partially performed through Special Coordination Funds of the Science and Technology Agency of the Japanese government.

### Acknowledgments

The author wishes to acknowledge Dr. T. Mitsuhashi of National Institute for Research in Inorganic

Materials and Mrs. S. Okaya, F. Muta and T. Koshiro of Rigaku Corporation for their valuable contributions.

### References

- [1] S. Yugo, T. Sato and T. Kimura: Appl. Phys. Lett, **46** (1985), 842.
- [2] G. A. Slack: J. Phys. Chem. Solids, **34** (1973), 321.
- [3] C. Wood: Appl. Phys. Lett., **47** (1985), 1232.
- [4] Y. Kumashiro, T. Mitsuhashi, S. Okaya, F. Muta, T. Koshiro, Y. Takahashi and M. Hirabayashi: J. Appl. Phys., **65** (1989), 2147.
- [5] Y. Kumashiro, T. Mitsuhashi, S. Okaya, F. Muta, T. Koshiro, Y. Takahashi, M. Hirabayashi and Y. Okada: High Temp.-High Press, **21** (1989), 105.
- [6] Y. Kumashiro, Y. Okada and S. Gonda: J. Crystal Growth, **70** (1985), 507.
- [7] J. Ohsawa, T. Nishinaga, and S. Uchiyama: Jap. J. Appl. Phys., **17** (1978), 1059.
- [8] T. Mizutani, J. Ohsawa, T. Nishinaga and S. Uchiyama: Jap. J. Appl. Phys., **15** (1976), 1305.
- [9] E. S. R. Gopal: Specific Heats at low Temperatures, Plenum Press, New York (1966).
- [10] T. Mitsuhashi, F. Muta, T. Chiba and Y. Fujiki: The Rigaku-Denki Journal 19, No. 2 (1988), 16.
- [11] D. A. Watt: Brit. J. Appl. Phys., **17** (1966), 231.
- [12] Y. Kumashiro, M. Hirabayashi and S. Takagi: Proc. Mat. Res. Soc., Diamond, Boron Nitride, Silicon Carbide and Related Wide Bandgap Semiconductors, Material Research Society, Pittsburgh, (1990) in print.
- [13] Y. Kumashiro, M. Hirabayashi, T. Koshiro and Y. Okada: J. Less-Common Metals, **143** (1988), 159.
- [14] J. E. Parrott and A. D. Stuckes: Thermal Conductivity of Solids, Pion, London (1975).
- [15] E. F. Steigmeier and L. Kudrnan: Phys. Rev., **132** (1963), 508.
- [16] Y. Kumashiro, M. Hirabayashi, T. Koshiro and Y. Takahashi: Sintering '87, Elsevier, London (1988) p. 43.